Random Walks with Adaptive Cylinder Flux Based Connectivity for Vessel Segmentation

Ning Zhu and Albert C.S. Chung

Lo Kwee-Seong Medical Image Analysis Laboratory,
Department of Computer Science and Engineering,
The Hong Kong University of Science and Technology, Hong Kong
{nzhu,achung}@cse.ust.hk

Abstract. In this paper, we present a novel graph-based method for segmenting the whole 3D vessel tree structures. Our method exploits a new adaptive cylinder flux (ACF) based connectivity framework, which is formulated based on random walks [8]. To avoid the shrinking problem of elongated structure, all existing graph-based energy optimization methods for vessel segmentation rely on skeleton or ROI extraction. As a result, the performance of these vessel segmentation methods then depends heavily on the skeleton extraction results. In this paper, with the help of ACF based connectivity framework, a global optimal segmentation result can be obtained without extracting skeleton or ROI. The classical issues of the graph-based methods, such as shrinking bias and sensitivity to seed point location, can be solved effectively with the proposed method thanks to the connectivity framework.

1 Introduction

Blood vessel disease is one of the major causes of death around the world. For treating the vessel diseases, segmentation technique has been playing an important role since it is an essential tool for diagnosis and treatment planning. A variety of vessel segmentation methods have been proposed in recent years [12].

Graph-based methods, such as graph cuts [4,5], random walks [8] and power-watershed [6] have become a group of widely used image segmentation methods because global optimal segmentation can be performed efficiently by energy minimization. Therefore graph-based methods have been extended in many applications and promising results have been shown in [9,14,16]. However graph-based segmentation methods cannot give superior performance on some specific medical applications, such as vessel segmentation which is a challenging task. For elongated structures, energy optimization methods can have the problem of shrinking bias [10,16]. This problem is usually solved by providing more seed points or structure skeletons. But with the advanced developments of 3D image acquisition techniques, image resolution increases significantly and it is difficult for users to provide many accurate seeds for vessels with large extension area. Besides, it is difficult to model the intensity change from the root to the distal parts. Sometimes the distal parts may be indistinguishable from the background

K. Mori et al. (Eds.): MICCAI 2013, Part II, LNCS 8150, pp. 550–558, 2013.

area since the intensity is low and similar. These specific issues set a barrier for using the graph-based methods despite of the advantages of those methods. As a result, there are not many graph-based methods [3,7,14,15,17] proposed for vessel segmentation. In [14,15,17], the optimization can be obtained only for single branches. Methods in [3,7] work for vessel tree structure by first extracting the skeleton and ROI before segmentation. All these graph-based methods depend on skeleton extraction, and the extraction errors can lead to fatal and irretrievable mistakes in the segmentation process.

Paper Contributions. We propose a new random walks based method for vessel tree structure segmentation with the help of adaptive cylinder flux (ACF) based connectivity. There are four superior properties of the proposed method. (i) With ACF, the connectivity for edges with high probability being in the vessel center and having the same direction with the vessel is embedded in the new objective function and it is evaluated to be effective in increasing the accuracy and reducing the adverse effect of shrinking bias. (ii) The optimization is done on the whole 3D image without extracting ROI. As a result, the performance of the proposed method does not depend on the skeleton extraction results. (iii) The global optimal segmentation result can be obtained. (iv) Bifurcations of vessel tree structure do not require extra consideration in our method.

2 Background

The proposed method is developed based on the random walks framework [8]. The basic definition and some equations of random walks will be described in this section. We define the undirected graph as $G = (V, E)$, in which V and E are node set and edge set respectively. w_{ij} is the weight assigned to the edge e_{ij}, and for undirected graph, $w_{ij} = w_{ji}$. In random walks [8], the combinatorial formulation of the Dirichlet integral for segmentation is defined as,

$$D[x] = \frac{1}{2}(Ax)^T C(Ax) = \frac{1}{2}x^T Lx = \frac{1}{2}\sum_{e_{ij}\in E} w_{ij}(x_i - x_j)^2, \tag{1}$$

in which L (combinatorial Laplacian matrix) and A (edge-node incidence matrix) are defined as,

$$L_{ij} = \begin{cases} d_i & \text{if } i = j; \\ -w_{ij} & \text{if } e_{ij} \in E; \\ 0 & otherwise. \end{cases} \quad and \quad A_{e_{ij},v_k} = \begin{cases} +1 & \text{if } i = k; \\ -1 & \text{if } j = k; \\ 0 & otherwise. \end{cases} \tag{2}$$

C is an edge-edge incidence diagonal matrix with the weights of edges along the diagonal direction. x_i is the probability for walkers starting from v_i first arrive at foreground seed v_s rather than background seed v_b, as a result, $x_{v_s} = 1$ and $x_{v_b} = 0$. The probabilities (or potentials in circuit) $x = (x_1, x_2 ... x_n)^T$ is estimated by minimizing $D[x]$, and then the label for each node v_i is determined according to x_i. d_i is the sum of w_{ij} for $e_{ij} \in E$.

3 Proposed Method

In this section, a new feature, namely adaptive cylinder flux (ACF), is first proposed for enhancing the edge connectivity. Then a new framework with

connectivity enhancement is defined for vessel segmentation based on random walks, and the method for the optimization of the new framework will also be described.

3.1 Adaptive Cylinder Flux

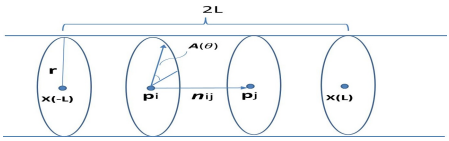

Fig. 1. Geometric Graph

In this section, adaptive cylinder flux (ACF) is proposed for enhancing the graph connectivity for random walks based segmentation of the whole vasculature. Inspired by [11], in which the flux through sphere is measured to determine whether a pixel is located near the tube center, we propose an adaptive cylinder flux as a feature to measure whether two neighboring pixels, for example, p_i and p_j in Fig. 1, are in a tube with the direction $\boldsymbol{n}_{ij}$ along the direction of the tube. First, the flux through cylinder side surface is defined as follows,

$$f(e_{ij}, r, \lambda) = \frac{1}{4\pi L} \int_{-L}^{L} \int_{0}^{2\pi} \boldsymbol{g}(x(l,\theta)) \cdot (-\boldsymbol{A}(\theta)) d\theta dl,$$

where $L = r \times \lambda (L > 0)$, $\boldsymbol{g}(\cdot)$ is gradient vector, and

$$x(l) = \frac{p_i + p_j}{2} + \boldsymbol{n}_{ij} \cdot l, \quad x(l,\theta) = x(l) + r\boldsymbol{A}(\theta), \quad \boldsymbol{n}_{ij} = \frac{(p_j - p_i)}{|p_j - p_i|}.$$

e_{ij} is an edge connecting two neighboring voxel v_i and v_j, and the coordinates of the two voxels are p_i and p_j. $\boldsymbol{A}(\theta)$ is the unit vector from the center point $x(l)$ to cylinder surface point on the cross section perpendicular to $\boldsymbol{n}_{ij}$ and with $x(l)$ on it, and we have $\boldsymbol{A}(\theta + \pi) = -\boldsymbol{A}(\theta)$. For measuring symmetry, we define a feature symmetric with the cross section centers,

$$s(e_{ij}, r, \lambda) = \frac{1}{2\pi L} \int_{-L}^{L} \int_{0}^{\pi} |(\boldsymbol{g}(x(l,\theta+\pi)) + \boldsymbol{g}(x(l,\theta))) \cdot \boldsymbol{A}(\theta)| d\theta dl.$$

For edges in a tube and with direction $\boldsymbol{n}_{ij}$ along the tube direction, $f(e_{ij}, r, \lambda)$ should be large and $s(e_{ij}, r, \lambda)$ should be small. Assume $flux(x(l,\theta)) = \boldsymbol{g}(x(l,\theta)) \cdot (-\boldsymbol{A}(\theta))$, we define the adaptive cylinder flux as,

$$\begin{aligned} ACF(e_{ij}) &= \max_r \{f(e_{ij}, r, \lambda) - s(e_{ij}, r, \lambda)\}, \\ &= \max_r \frac{1}{2\pi L} \int_{-L}^{L} \int_{0}^{\pi} \min(flux(x(l,\theta+\pi)), flux(x(l,\theta))) d\theta dl. \end{aligned} \tag{3}$$

This feature is adaptive since the length of cylinder changes according to the tube radius. λ is a constant value so here in function ACF we omit it and use $ACF(e_{ij})$ for short. Random walks is a graph-based method and we give a discrete version of ACF, named as $DACF$,

$$DACF(e_{ij}) = \max_r\{\frac{1}{4L'N}\sum_{l=-L'}^{L'-1}\sum_{k=0}^{2N-1}\boldsymbol{g}(x'(l,\frac{\pi k}{N}))\cdot(-\boldsymbol{A}(\frac{\pi k}{N}))$$

$$-\frac{1}{2L'N}\sum_{l=-L'}^{L'-1}\sum_{k=0}^{N-1}|(\boldsymbol{g}(x'(l,\frac{\pi k}{N}))+\boldsymbol{g}(x'(l,\frac{\pi k}{N}+\pi)))\cdot\boldsymbol{A}(\frac{\pi k}{N})|\}, \quad (4)$$

$$=\max_r\{\frac{1}{2L'N}\sum_{l=-L'}^{L'-1}\sum_{k=0}^{N-1}\min\{flux(x'(l,\frac{\pi k}{N})), flux(x'(l,\frac{\pi k}{N}+\pi))\}\},$$

where $L' >= 1$ and,

$$L' = \lfloor\frac{r\times\lambda}{|p_i-p_j|}+0.5\rfloor, \quad x'(l,\theta) = \frac{p_i+p_j}{2}+(l+0.5)\times(p_j-p_i)+r\boldsymbol{A}(\theta).$$

It is noted that the discrete ACF can be viewed as an extension of *Mflux* [13], in which only one cross section is considered. The length of the cylinder is changed adaptively according to the tube radius. In an extreme case, when $L' = 1$, two cross sections with v_i and v_j are considered. $f(e_{ij})$ itself can be used to detect tube with uniform intensity background. However, $f(e_{ij})$ may be very large for the nodes near the boundary of organs without vessel. While ACF can have a good response of vessels near organ boundary and its value is around zero for the nodes near boundary without vessel. Meanwhile, since the proposed feature considers the adaptive length of the vessel, it should be more robust to noise.

3.2 *ACF* Connectivity Enhanced Random Walks

Random walks [8] is designed for segmentation on 2D and 3D images. However, for vessel segmentation, the vessel points far from vessel seed v_s may have low probability to reach the v_s first because of the intensity change along the vessel. As a result, those points may be labeled wrongly as background. In this paper, we propose a new connectivity enhanced framework (Equation 5) based on the random walks framework so as to solve the problem for vessel segmentation.

$$x = \arg\min_x D[x] = \arg\min_x \frac{1}{2}(\sum_{e_{ij}\in E_o} w_{ij}(x_i-x_j)^2 + \sum_{e_{ij}\in E_{rg}} c_{ij}(x_i-x_j)^2),$$
$$\text{s.t. } x(v_s)=1,\ x(v_b)=0. \quad (5)$$

Here $G_{rg} = \{V_{rg}, E_{rg}\}$ is $DACF$ growing graph, $c_{ij} = \delta\cdot DACF(e_{ij})$, v_s and v_b are the vessel and background seeds. Actually, given v_s, v_b can be detected automatically, as a result, only seed point v_s near the root of the tree is essential. To construct a good vessel connectivity graph, $DACF$ based growing is first used to construct the graph G_{rg}, and this graph is merged with the 3D lattices (G_o) constructed by all voxels in the image by summing up the weights of the corresponding edges in G_{rg} and G_o. The method for constructing the new graph is described as Algorithm 1, in which $G_o = (V_o, E_o)$, V_o is the set of voxels in I, E_o includes edges connecting neighboring voxels in I, β is a parameter for calculating weights, τ is a threshold for $DACF$ region growing, I_i is the intensity of voxel v_i in I.

Algorithm 1. *DACF* Based Connectivity Enhanced Graph Construction

INPUT: I – image voxels, v_s – vessel seed, v_b – background seed.
INITIALIZATION: $V_{rg} = v_s, E_{rg} = \phi, Array = \{v_s\}$.
while $Array! = \phi$ **do**
  Pop one node v_i from Array.
  for each neighbor voxel v_j of v_i **do**
    if $v_j \notin V_{rg}$ **then**
      calculate $DACF(e_{ij})$ with Equation 4, e_{ij} is the edge connecting v_i and v_j.
      if $DACF(e_{ij}) \geq \tau$ **then**
        add v_j into $Array$ and V_{rg}, add e_{ij} into E_{rg}.
$G = G_o$, calculate $W_o = \{w_{o_{ij}} = \exp(-\beta(I_i - I_j)^2)\}$.
for $e_{ij} \in E_o$ **do**
  if $e_{ij} \in E_{rg}$ **then** $w_{ij} = w_{o_{ij}} + c_{ij}$
  else $w_{ij} = w_{o_{ij}}$
$W = \{w_{ij}\}$
OUTPUT: G and W

After obtaining the new graph G and W, the optimization of Equation 5 can be performed same as the optimization of Equation 1. Similar with the method in [8], the Equation 1 is decomposed into,

$$D[x_U] = \frac{1}{2}\begin{bmatrix} x_M^T & x_U^T \end{bmatrix}\begin{bmatrix} L_M & B \\ B^T & L_U \end{bmatrix}\begin{bmatrix} x_M \\ x_U \end{bmatrix} = \frac{1}{2}(x_M^T L_M x_M + 2x_U^T B^T x_M + x_U^T L_U x_U),$$

x_M and x_U here correspond to the potentials of seeded and unseeded nodes, respectively. Here we omit the definitions of other variables due to the space limitation. Please refer to [8] if needed. By differentiating $D[x_U]$ with respect to x_U, we may have $L_U x_U = -B^T x_M$. Then to obtain x_U, we use conjugate gradient method for solving the linear system since it is difficult to solve it directly due to the large size of L_U. It is obvious that the objective function (Equation 5) can be optimized with the proposed method. Random walks and electrical circuit works similarly in some respects, here we give a circuit theory interpretation of the proposed method.

Circuit Theory Interpretation: Since all complex circuits can be simplified to an equivalent simple circuit, here we just take the simple circuit in Fig. 2 as an example. In the circuit (Fig. 2), the voltages in the two ends are fixed, with $voltage(v_s) = 1$ and $voltage(v_b) = 0$, the segmentation is then equal to labeling the nodes with voltage greater than 0.5 to foreground object and background otherwise. According to the circuit theory, adding new resistor (new edge weight of connectivity) between v_i and v_j can also be interpreted as increasing the conductance of R_{ij} from original conductance $w_{o_{ij}}$ to $w_{ij} = w_{o_{ij}} + c_{ij}$. This procedure is similar with the graph merging procedure of Algorithm 1. According to the Ohm's law ($I \cdot R = V$), if the voltage V is fixed, decreasing the resistivity R can cause the current I increased. As a result, in the circuit of Fig. 2, adding a new resistor between v_i and v_j can cause the voltage of v_j increased, and similarly the probability of the v_j being foreground object will be increased. Therefore, enhancing connectivity for the edges in E_{rg} can lead to the sequentially increase of the potentials for the nodes covered by the *DACF* based growing. Similarly, in the perspective of the random walks, increasing the weights of these edges can increase the probability of the walkers to walk across the edges in E_{rg}.

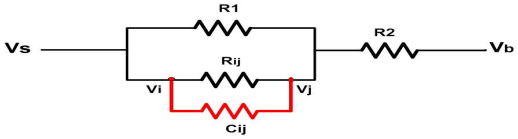

Fig. 2. Circuit Interpretation

4 Experiments

For evaluation, we have compared the proposed method with other closely related segmentation methods on both synthetic images and clinical images. First, a group of experiments have been carried out on synthetic tree (Fig. 3(a)) and synthetic tube (Fig. 3(c)) with intensity and radius change. Gaussian noise was added to generate a series of noisy synthetic images for evaluation.

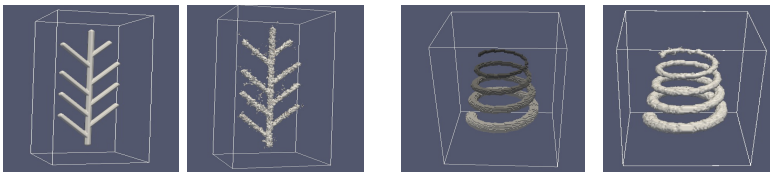

Fig. 3. Experiments on Synthetic Images: (from left to right: Synthetic Image 1, proposed method result ($\sigma = 400$), Synthetic Image 2, proposed method result($\sigma = 200$))

The proposed method was compared with the random walks [8], power-watershed method [6] and graph cuts [4] on two groups of synthetic images. We have also performed a comparison with the power-watershed and graph cuts method by providing the same connectivity enhanced graph obtained with the proposed method. For evaluating the segmentation accuracy, the percentage of voxels being labeled correctly is not an ideal measure, so we employ a widely used statistic measure, namely F-measure (or F-Score) with $\alpha = 1$, which is equivalent to Dice Coefficient.

Table 1. F-1 Score (DICE) on Synthetic Image 1

σ (noise level)	**WithoutNoise**	100	200	300	400
Our method	100%	96.88%	95.19%	90.66 %	88.43%
WaterShed [6]	99.99%	97.80%	10.03%	1.76%	1.76%
GraphCut [4]	100%	98.01%	14.76%	0.02%	1.74%
RandomWalks[8]	100%	98.29%	92.32%	76.04%	54.73%
WaterShed with *DACF*	100%	97.93%	83.09%	35.82%	1.41%
GraphCut With *DACF*	100%	98.98%	1.74%	1.32%	1.32%

By providing reasonable edge connectivity based on $DACF$, which can reduce the shrinking risk, the proposed method can have good performance on noisy images, as can be seen in Table 1 and Table 2. Fig. 3(b) and 3(d) show the surface obtained with the proposed method for noisy images with $\sigma = 400$ and $\sigma = 200$. The accuracy of the other methods drops quickly as the noise level increases. For graph cuts method, $DACF$ connectivity cannot help to avoid shrinking to the background seed or a small number of voxels near the seed.

Table 2. F-1 Score (DICE) on Synthetic Image 2

σ (noise level)	**WithoutNoise**	80	100	200	300
Our method	100%	100%	97.58 %	92.42 %	79.20%
WaterShed [6]	100%	100%	91.54%	4.71%	4.71%
GraphCut[4]	100%	100%	95.49%	4.78%	4.79%
RandomWalks[8]	100%	100%	73.14%	49.52%	24.21%
WaterShed with $DACF$	100%	100%	99.62%	4.83%	4.83%
GraphCut With $DACF$	100%	100%	99.79%	4.78%	4.78%

The performance of Watershed method can be better with $DACF$ connectivity. However, the method emphasizes too much on edge cost and the unpredictable intensity changes in noisy image can cause the power-watershed to build "dam" and make the segmentation result unpredictable. Different from maximum-flow, which assumes x as integers 0 or 1, random walks and the proposed method regard the resulting label x in Equation 1 as a real number ranges from 0 to 1. As a result, x for neighboring voxels with high connectivity will always have similar values. So the segmentation never shrinks to seed points and F-score for random walks does not drop to very low value with $DACF$ connectivity. In all experiments, the weight λ for calculating $DACF$ was set to 1.5. β in Algorithm 1 was set to 0.005 in the synthetic experiments and 0.05 for the real

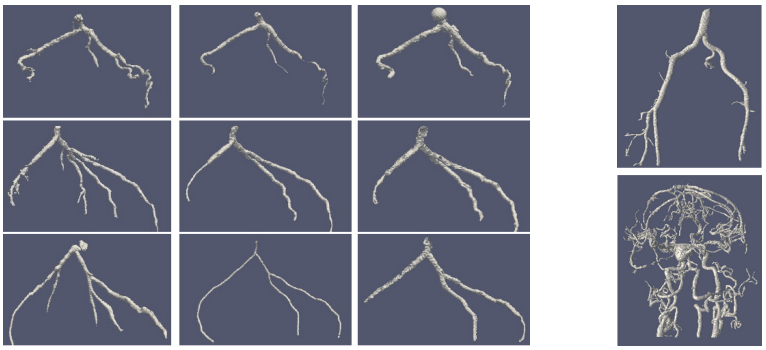

(a) Comparision on CTA images (from left to right: our method, results from [3] and [7])

(b) Results on MRA

Fig. 4. Experiments on Clinical CTA and MRA Images

images because this parameter is closely related to boundary intensity change. τ was set to 100 for synthetic images, 40 for CTA and 60 for MRA images. δ for calculating c_{ij} set to 0.02.

Due to the difficulty of obtaining the ground truth segmentation for whole vessel tree structures, we conduct the experiments on clinical images and compare the methods qualitatively. The proposed method is first compared with two up-to-date graph-based vessel segmentation methods [3,7] on clinical CTA images from Rotterdam Framework([1] with permission) for coronary artery segmentation(Fig. 4(a)). The experiments are carried out on a number of CTA images. Due to the space limitation, we only present the experiment results on 3 images here. The experiment is also done with power-watershed [6] and graph cuts methods. However, the segmentation results shrink to small areas near the background seed, so we do not present the results here. For method in [3,7], the centerlines of three major vessels are first detected and the voxels with their smallest distance to any centerline points within 1.5 radius are assumed as candidate voxels. For the proposed method, power-watershed method, and graph cuts method, only a vessel seed point and a background point near it are provided. As shown in the figure, good segmentation results for the tree structure can be obtained with the proposed method without using vessel skeleton or ROI, and it does not suffer from shrinkage to centerline points as [3] does. In the experiments for all methods, to avoid leakage to heart, a "block" is built in CTA images only with the help of the provided vessel seed near the root of the vascular tree.

Some experiments are also carried out on MRA images from OsiriX [2] and the segmentation results of lower limbs vessels and cerebral vessels are presented in Fig. 4(b). From the figure we can see that good segmentation results can be obtained with the proposed method, and the issue of intensity brightness near boundary for MRA images can be resolved by finding maximal ACF response for different radii.

5 Conclusion

In this paper, we have presented a novel graph-based segmentation method for 3D vessel tree structures. Our method exploits a new adaptive cylinder flux (ACF) based connectivity framework, which is formulated based on random walks [8]. With the help of the ACF based connectivity framework, a global optimal segmentation result can be obtained without extracting skeleton or ROI. The proposed method has been compared with classical graph-based image segmentation methods and two up-to-date 3D vessel segmentation methods and promising results have been reported on both CTA and MRA images.

We would like to acknowledge the financial support of the Hong Kong Research Grants Council under grant 612011.

References

1. http://coronary.bigr.nl/centerlines/rules.php
2. http://www.osirix-viewer.com/datasets/
3. Bauer, C., Pock, T., et al.: Segmentation of interwoven 3d tubular tree structures utilizing shape priors and graph cuts. MedIA 14(2), 172–184 (2010)
4. Boykov, Y., Funka-Lea, G.: Graph cuts and efficient nd image segmentation. IJCV 70(2), 109–131 (2006)
5. Boykov, Y., Jolly, M.: Interactive graph cuts for optimal boundary & region segmentation of objects in nd images. In: ICCV, vol. 1, pp. 105–112 (2001)
6. Couprie, C., Grady, L., et al.: Power watershed: A unifying graph-based optimization framework. PAMI 33(7), 1384–1399 (2011)
7. Esneault, S., Lafon, C., et al.: Liver vessels segmentation using a hybrid geometrical moments/graph cuts method. IEEE Trans. on BME 57(2), 276–283 (2010)
8. Grady, L.: Random walks for image segmentation. PAMI 28(11), 1768–1783 (2006)
9. Hanaoka, S., Fritscher, K., Welk, M., Nemoto, M., Masutani, Y., Hayashi, N., Ohtomo, K., Schubert, R.: 3-D graph cut segmentation with riemannian metrics to avoid the shrinking problem. In: Fichtinger, G., Martel, A., Peters, T. (eds.) MICCAI 2011, Part III. LNCS, vol. 6893, pp. 554–561. Springer, Heidelberg (2011)
10. Kolev, K., Cremers, D.: Continuous ratio optimization via convex relaxation with applications to multiview 3d reconstruction. In: CVPR, pp. 1858–1864 (2009)
11. Law, M.W.K., Chung, A.C.S.: An oriented flux symmetry based active contour model for three dimensional vessel segmentation. In: Daniilidis, K., Maragos, P., Paragios, N. (eds.) ECCV 2010, Part III. LNCS, vol. 6313, pp. 720–734. Springer, Heidelberg (2010)
12. Lesage, D., Angelini, E., et al.: A review of 3D vessel lumen segmentation techniques: Models, features and extraction schemes. MedIA 13(6), 819–845 (2009)
13. Lesage, D., Angelini, E., et al.: Design and study of flux-based features for 3D vascular tracking. In: ISBI, pp. 286–289 (2009)
14. Li, K., Wu, X., et al.: Optimal surface segmentation in volumetric images-a graph-theoretic approach. PAMI 28(1), 119–134 (2006)
15. Schaap, M., van Walsum, T., et al.: Robust shape regression for supervised vessel segmentation and its application to coronary segmentation in CTA. TMI 30(11), 1974–1986 (2011)
16. Vicente, S., Kolmogorov, V., Rother, C.: Graph cut based image segmentation with connectivity priors. In: CVPR, pp. 1–8 (2008)
17. Zhao, F., Zhang, H., et al.: Congenital aortic disease: 4D magnetic resonance segmentation and quantitative analysis. MedIA 13(3), 483–493 (2009)